

NJC

Accepted Manuscript



This is an *Accepted Manuscript*, which has been through the Royal Society of Chemistry peer review process and has been accepted for publication.

Accepted Manuscripts are published online shortly after acceptance, before technical editing, formatting and proof reading. Using this free service, authors can make their results available to the community, in citable form, before we publish the edited article. We will replace this *Accepted Manuscript* with the edited and formatted *Advance Article* as soon as it is available.

You can find more information about *Accepted Manuscripts* in the [Information for Authors](#).

Please note that technical editing may introduce minor changes to the text and/or graphics, which may alter content. The journal's standard [Terms & Conditions](#) and the [Ethical guidelines](#) still apply. In no event shall the Royal Society of Chemistry be held responsible for any errors or omissions in this *Accepted Manuscript* or any consequences arising from the use of any information it contains.



www.rsc.org/njc



NJC

PAPER

Hydrogen-gas sensors based on graphene functionalized palladium nanoparticles: the impedance response as a valuable sensor evaluation†

Received 00th January 20xx,
Accepted 00th January 20xx

DOI: 10.1039/x0xx00000x

www.rsc.org/

Reinaldo David Martínez-Orozco,^{*a} René Antaño-López^b and Vicente Rodríguez-González^a

Palladium-graphene nanostructures (PdGO) with high-quality-graphene layers and well monodispersed palladium nanoparticles (PdNPs) were synthesized by the hydrothermal microwave exfoliation method. The structural and morphological characteristics of PdGO were investigated, and the results indicate that the hydrothermal-microwave method allows both the reduction of the metal precursors and their anchorage on highly exfoliated graphene layers. The synthesized PdGO was then deposited as active layers for sensing hydrogen gas (H₂). PdGO-based sensors with gas concentrations from 0.01 to 5 vol. % in air exhibited a very reproducible performance with fast response times (~30 seg) and recovery behavior at room temperature. Impedance response results as a high sensitive feasible sensor technique. Our results show that it is feasible to obtain an efficient H₂-sensor with reliable and reproducible sensing properties by means of a simple and cost-effective preparation method under real atmospheric conditions.

1. Introduction

Hydrogen (H₂) is considered as an ideal fuel due to its high-energy content and clean nature. It has a great potential as an energy option in many industrial and technological applications. Its combustion in air produces only water and it is a common element on the earth: it is present in water, biomass and hydrocarbons.^{1,2} The promising use of H₂ can help meet the always growing energy demand; however, in order to implement it, H₂ monitoring and leak detection systems are required because it is invisible, odorless and highly flammable. At concentrations above 4 vol. % in air, H₂ is flammable, and explosive in a wide range of concentrations (15-59%) at normal atmospheric pressure.³

The common hydrogen-gas sensors based on metal-oxides such as SnO₂,⁴ In₂O₃,⁵ ZnO,⁶ NiO,⁷ and TiO₂,⁸ have shown appropriate sensitivities, however, from the power consumption point of view, they may not be favorable due to their operation at high temperatures. Currently, palladium-hydrogen (Pd-H₂) systems are a key issue in several applications such as hydrogen storage, hydrogenation process and detection.¹ Palladium (Pd) is an attractive material for the detection of H₂ due to its high hydrogen solubility at room temperature, but hydrogen sensors based on

palladium materials may be vulnerable to structural changes due to the formation of palladium hydride (PdH_x).⁹ Two PdH_x phases can occur: Pd_α-phase (solid solution of Pd and H) and Pd_β-phase (Pd hydride). By increasing the hydrogen concentration, which is incorporated into palladium, the phase transition from Pd_α to Pd_β occurs, causing irreversible expansion and mechanical damage.¹⁰ This phenomenon can modify the H₂ diffusion coefficient, affecting the response and recovery, particularly at either low or high concentrations.¹¹ One of the current approaches for overcoming these drawbacks is to conduct research on several palladium nanostructures such as nanowires,^{12,13} nanotubes¹⁴ and composite materials,¹⁵ in order to get a better performance in terms of sensitivity, time response and stability.

On the other hand, current methods to obtain graphene-based materials allow the synthesis of new hybrid materials such as metallic-nanoparticles-carbon-materials systems, thus providing greater chances to obtain nanostructured materials for sensor applications. Johnson et al. have reported the detection of hydrogen at room temperature with fast response and recovery times, from graphene-nanoribbon porous films decorated with Pd.¹⁶ Mubeen et al. showed the application of porous films of carbon nanotubes decorated with Pd in the detection of hydrogen.¹⁷ In the same context, Cui et al. reported on AgNP-decorated-reduced graphene oxide and its applications in the detection of ammonia,¹⁸ while Prezioso et al. described the detection of NO₂ by only using graphene oxide, indicating that the sensing properties are mediated by oxygenated functional groups.¹⁹

The works mentioned above shows that the incorporation of nanoparticles and the presence of functional groups on graphene layers play a significant role in the detection of gases.¹⁵⁻¹⁹ The

^a División de Materiales Avanzados, Instituto Potosino de Investigación Científica y Tecnológica, Camino a la Presa San José 2055 Col. Lomas 4a. sección C.P. 78216, San Luis Potosí, S.L.P., México. E-mail address: reinaldo.martinez@ipicyt.edu.mx; Tel. +52 4448342000

^b Centro de Investigación y Desarrollo Tecnológico en Electroquímica, S.C., Pedro Escobedo, Querétaro, México.

† Electronic Supplementary Information (ESI) available: EDX analysis, Raman and FTIR spectra, additional SEM images of PdGO, concentration determination, raw data and reproducibility test in hydrogen detection. See DOI: 10.1039/x0xx00000x

oxygen functional groups can act as active sites for interacting with gaseous molecules, but may also affect the sensor response by a sluggish and irreversible recovery, which makes them unable to produce a reproducible and reliable signal detection.²⁰ Hybrid materials such as carbon-metal nanoparticles are beneficial in several ways: (i) graphene layers tend to be re-stacked by removing functional groups, and it is worth pointing out that interlayer-spacing is a critical issue to obtain functional materials. An adequate separation prevents the formation of re-stacked graphene layers and maintains the surface area, providing the necessary diffusion of molecules or ions to be detected, and (ii) metallic nanoparticles are ready to aggregate due their high surface energy, which leads to decrease the number of accessible sites and hence to degrade the catalytic activity.²¹ So, 2D carbon materials are attractive as nanoparticle supports, which allow to improve their dispersion, whilst the incorporation of nanoparticles (NPs) into graphene layers preserves the spacing and prevents them from being re-stacked.²² Finally, a characteristic of nanoscale materials, in comparison with their bulk counterparts, is their high surface-to-volume ratio, which favors the adsorption of gas onto the sensor, enabling an increase in the device sensitivity, where the interaction between the gas of interest and the sensor active layer is increased.²³

In this study, the preparation of a hydrogen-gas sensor prototype based on Pd nanoparticles dispersed and anchored on graphene layers, synthesized by the microwave method, is reported. The employed methodology allows the synthesis of functional palladium-graphene nanostructures. Our experimental detection results exhibited a very reproducible performance with fast response times and recovery properties at room temperature. All the hydrogen-sensor studies were carried out under air stream at room temperature and different H₂ concentrations from 0.01 to 5 vol. %.

2. Experimental

2.1 Synthesis

The synthesis of palladium-graphene nanostructures (PdGO) was performed by the microwave method reported by Il-Kwon Oh's group.^{24,25} Firstly, expandable graphite oxide was prepared from natural powder graphite (Sigma Aldrich, <150 μm, 99.99 %) by a modified Hummers method.²⁶ After filtering, multiple washing and drying, 0.5 g of expanded graphite oxide were dispersed in ethanol and 0.3 g of Palladium(II) acetylacetonate (Pdacac, Sigma Aldrich, 99%) and 0.30 mL of 1-Butyl-3-methylimidazolium tetrafluoroborate (EMIM-BF₄, Sigma Aldrich) were added and ultrasonicated (Branson, 42 KHz, 230 W) for 30 min. Later, the mixture was subjected to three consecutive cycles of microwave irradiation (ETHOS, Milestone, ~700 W) for about 10 minutes. The metal loading was calculated to be 20 wt. % with respect to carbon. The as-resulting-palladium-nanoparticles-graphene nanostructures were later used in active layers for hydrogen-gas detection. The composite is referred to as PdGO because graphene was synthesized from wet chemical methods. CAUTION: Temperature must be controlled carefully in order to avoid any reactions between the synthesized material and Teflon-lined containers.

2.2 Sensor preparation

The sensors were made in the configuration of two electrodes on glass substrates (10x10 mm). First, the substrates were cleaned with successive washes in acetone, methanol and deionized water for 15 min at room temperature. The synthesized PdGO was dispersed in water by ultrasonic treatment to produce a stable suspension at a concentration of 25 mg/mL, to which PVA (MW 1500 at 2%) was added to improve the dispersion. Two copper tapes (3M Conductive Copper Tape) were placed with a space of less than 2 mm. The deposition of the PdGO active layer was carried out by adding 60 μL dropwise of the synthesized material suspension to close the circuit between the tapes, and the prepared devices were dried at 80 °C overnight. The evaporation of water caused the formation of an active layer film which covered the space between the copper strips.

2.3 Sensor testing

Hydrogen-sensing tests were carried out by measuring the impedance response of the prototype sensors, which were placed inside a Teflon sealed chamber with a volume capacity of 100 mL (see Figure 1). A bias voltage fixed at 1 V was applied to the electrodes and the impedance value was registered with a Bio-Logic VSP-300 potentiostat in PEISW mode (potentiostatic setting). The sensor was subjected to exposure cycles that comprise 0.0, 0.01, 0.1, 0.5, 1.0, 3.0 and 5 vol. % of hydrogen. A gas mixture stream was delivered at a constant flow of 100 sccm (standard cubic centimeters per minute) and the H₂ concentration was controlled by its amount in the mixture with synthetic air. Initially, the sensor was allowed to stabilize under bias voltage and once stable response was reached, the as-prepared gas sensor was tested under the following test sequence: (1) synthetic air flowed through the chamber to obtain a stable baseline, (2) then hydrogen gas was injected into the air stream to detect the signal of interest and (3) the sensor test chamber was purged with air only for the sensor recovery. The duration of each step was 10 min for detection and 20 min for recovery. The test sequence was performed six times and the sensor response was calculated from these data. All the tests were performed under the following atmospheric conditions: temperature: 24° ± 2°C, pressure: 1.0 ± 0.05 bar, constant gas flow rate: 100 ± 2 sccm and atmospheric relative humidity: 50% ± 10%.

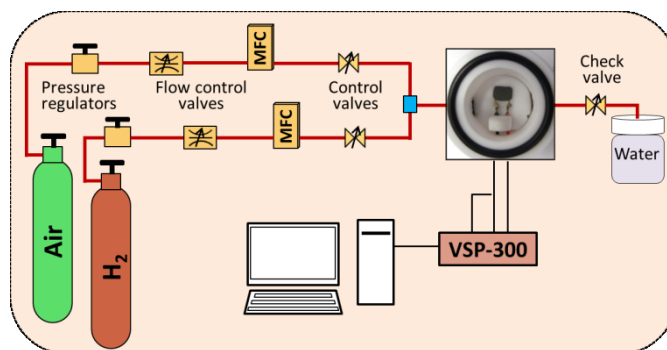


Fig. 1 Schematic representation of the experimental setup used for hydrogen gas detection.

2.4 Characterization of the material

Powder X-ray diffraction (XRD) was used to examine the phase and structure of the material. The XRD patterns were recorded between 5 and 80° (2 θ) with a Bruker D8 X-ray diffractometer with Cu K α radiation ($\lambda = 1.54 \text{ \AA}$) and a step of 0.02°. The morphology and structure of the synthesized materials were characterized by scanning electron microscopy in a Helios NanoLab 600i microscope with field emission for high-resolution images. Backscattered electron images (BS-SEM) were obtained by means of a Quanta 200 microscope with tungsten filament. The elemental composition of the material was determined by energy dispersive X-ray spectroscopy (EDS) with a spectrometer installed in the SEM EDAX. The transmission electron microscopy (TEM) and high resolution images TEM (HRTEM) of the materials were captured using an ultra-high resolution field emission electron microscope (FEI Tecnai at 300kV). Vibrational properties were identified by means of a Raman spectrometer (Micro-Renishaw) with a 514-nm excitation green laser. Fourier transform infrared spectra (FTIR) were performed to analyze the functional groups incorporated into the carbon material (Thermo Nicolet 6700). Electrochemical impedance spectra and H $_2$ -detection tests were performed with a potentiostatic/galvanostat system (VSP-300, Bio-logic), wherein reference and counter electrodes were connected together to the first sensor terminal, while the other was connected to the working electrode (Fig. 1).

3. Results and discussion

3.1 Material characterizations

Expanded graphite oxide can be an excellent precursor for the synthesis of graphene materials at feasible prices. This chemical graphene derivative is commonly prepared by an acid intercalation/exfoliation process in solution. This approach involves the delamination of the graphite crystal to reduce its thickness until individual graphene layers are obtained. One of their advantages in

comparison with pristine graphene lies in the presence of functional groups, which allows them to remain exfoliated in polar solvents. The as-expanded graphite oxide prepared by a modified Hummers method was characterized and Figure 2 summarizes these results. The stacking of graphene layers in the c-axis direction has been studied commonly as a function of the intercalation/exfoliation process during the synthesis of graphite oxide. The position of the reflection peaks (002) of graphite corresponds to the average distance between carbon layers (d_{002}), and this interlayer distance is 3.34 \AA . In contrast, graphite oxidation led to the shift and occurrence of broad-diffraction peaks at 11.3 and 42.5 in 2-theta. This interlayer expansion was calculated with $d_{002} = 7.8 \text{ \AA}$ by the Bragg law, which is larger than of the original graphite, confirming the expansion and exfoliation of the graphene layer in the c-axis direction, which were produced by the incorporation of oxygenated functional groups into the graphene layers. This increase in interlayer distance allowed the exfoliation that produced graphene oxide in aqueous media through the ionization of incorporated functional groups.²⁷ Figure 2b shows a representative image of the as-prepared GO layers. The GO layers look very thin with only the edges partially folded. This is a characteristic morphology resulting from their exfoliation, which normally occurs in a turbostratic way. Also, a crumpled structure is observed due to possible agglomerations of exfoliated sheets which are attributed to π - π interactions when the sample is dried. Ideally, one would expect monolayers, but we observed few graphene layers of micron size. This result indicates that the intercalation/exfoliation process of graphite can reduce its thickness up to individual graphene layers. The corresponding EDX analysis of GO shows that it has a C:O weight ratio of 77:21, suggesting the presence of not highly oxidized graphite.²⁸ EDX results are shown in Fig. S1 (Supporting Information).

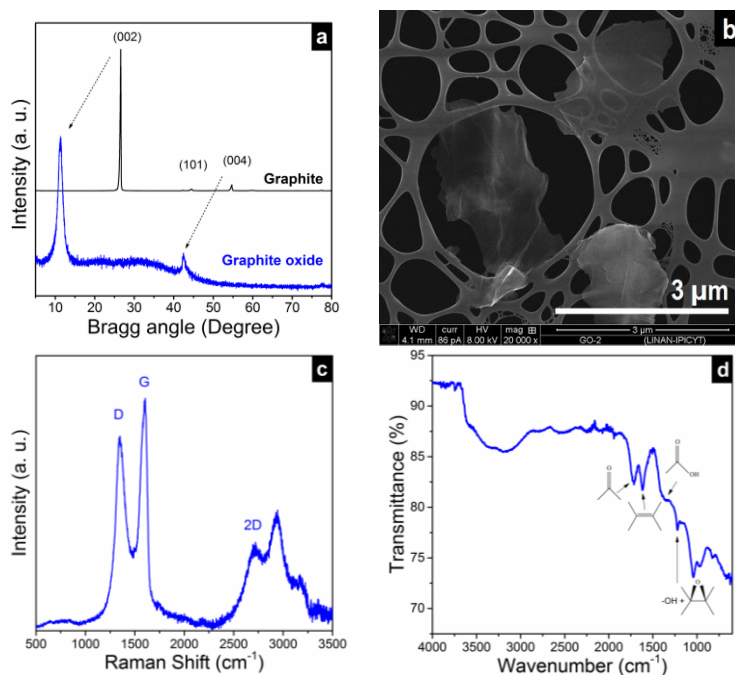


Fig. 2 (a) XRD patterns of expanded graphite oxide. (b) Typical SEM images of graphene oxide layers which reveal their wrinkled morphology. (c) Raman spectra of dried graphite oxide and (d) Transmission FTIR spectra of dried graphite oxide.

The Raman spectrum of GO (Figure 2c) shows the characteristic D and G bands of carbon materials. The D band is a characteristic feature for sp^3 domains in carbon layers and the G band provides information on the in-plane vibrations of sp^2 C-C bonds.²⁹ These two bands are present in GO, indicating that the sample contains both crystalline and amorphous carbon forms. The intensity of the D band is lower than of the G band, which could indicate a higher proportion of the carbon crystalline phase in GO. In addition, the G band is not broadening either, suggesting few plane defects. The broadening of the D band is due to the increased dispersion of stretching-bond frequencies stemming from the addition of functional groups. These results are in good agreement with the elemental analysis, which indicates a mild graphite oxidation that was enough to exfoliate its layers.

The presence of oxygen functional groups in the graphite oxide was corroborated by Fourier transform vibrational spectroscopy (FTIR). As shown in Figure 2d, the GO spectrum displays the broad O-H stretching in the $3700\text{--}2400\text{ cm}^{-1}$ region, and the presence of abundant oxygen groups such as carboxyl groups (C=O) at 1723 cm^{-1} , hydroxyl species at around 1400 and 1235 cm^{-1} (OH deformation and C-OH stretching) and epoxy species at 1050 and 820 cm^{-1} (C-O-C stretching).^{30,31} These functional groups have the effect of modifying the interlayer spacing of graphite oxide by reducing the π - π interactions between successive graphene layers.

The structure and surface chemistry of GO strongly depends on the oxidation level because the domain size of sp^2 carbon and density of the functional groups are affected by the oxidation extent. Actually, the production of large graphene sheets with few defects and few graphene layers is a great challenge. Graphene-resolution-processable methods such as the chemical routes are typically carried out by acid intercalation, but this intercalation process requires an oxidant. This approach involves concurrent processes such as intercalation, oxidation, exfoliation and graphite oxide formation.³² During this reaction, the cationic states induced in the graphite intercalation compound (GIC) are transformed into oxygenated groups by water attack during quenching.³³ In this work, a mild oxidation of graphite we performed, promoting the intercalation process and minimizing the oxidation by decreasing the amount of the oxidizing agent with prolonged stirring times. Also, the addition of water was carried out carefully to avoid high-temperature hydrolysis. Once the expanded GO was obtained, we proceeded to the synthesis of functional palladium-graphene nanostructures.

The characterization results of the as-obtained PdGO nanostructured sample synthesized by the hydrothermal microwave exfoliation method are shown in Figure 3. The image of the secondary electron (Fig. 3a) provides information about the surface morphology of PdGO, which confirms the successful functionalization of graphene layers with palladium nanoparticles performed by the microwave-assisted method. The obtained images show that PdGO consists of a few micron-sized-graphene layers, highly decorated by palladium nanoparticles anchored on carbon structures. The backscattered-electron analysis (Fig. 3b) confirmed the uniform distribution of palladium particles onto

graphene layers and the elemental analysis (EDX) of the sample endorsed its chemical composition. The percentage level of PdNPs (~20 wt. %) depends on the performed synthesis as it can be seen in Fig. 3c. In addition, the oxygen signal was decreased in all the analyzed regions, indicating the removal of oxygen functional groups, which is consistent with the reduction of graphene oxide. The obtained diffraction pattern of PdGO consists of a set of seven peaks: five peaks at 2θ angles of 40.1 , 46.6 , 68.1 , 82.0 and 86.4° corresponding to Pd nanoparticles crystallized in a face-centered cubic structure (fcc) (JCPDS 46-1043), and two peaks at about 26 and 55° , exhibit the presence of a slightly-layered graphene. The average particle size of palladium was calculated from the peak width of reflection (111) using the Scherrer-equation and the resulting value was 56 nm . The Raman spectrum shows that the PdNPs produced an additional intensity increase in the D peaks in PdGO in comparison with only GO, but the width of both D and G peaks remained unchanged (Fig. S2a, Supporting Information). In addition, the FTIR results corroborated the removal of functional groups in PdGO, which is consistent with EDX results, indicating a successful reduction of GO (Fig. S2b).

The reduction and functionalization of GO is a synergistic process. Under microwave irradiation, the presence of oxygenated groups —with negative charge— on GO, can favor the interaction with metal cations and serve as nucleation and growth sites of Pd nanoparticles.³⁴ On the other hand, Pd^{2+} cations can be reduced by ionic liquid due to their reducing properties, and graphene layers are exfoliated by either microwave radiation or catalytic activity of EMIM-BF₄. Also, EMIM-BF₄ and Pdacac by-products can produce carbonaceous gases that can serve as a carbon source for the successful reduction of GO (Fig. S3, Supporting Information).

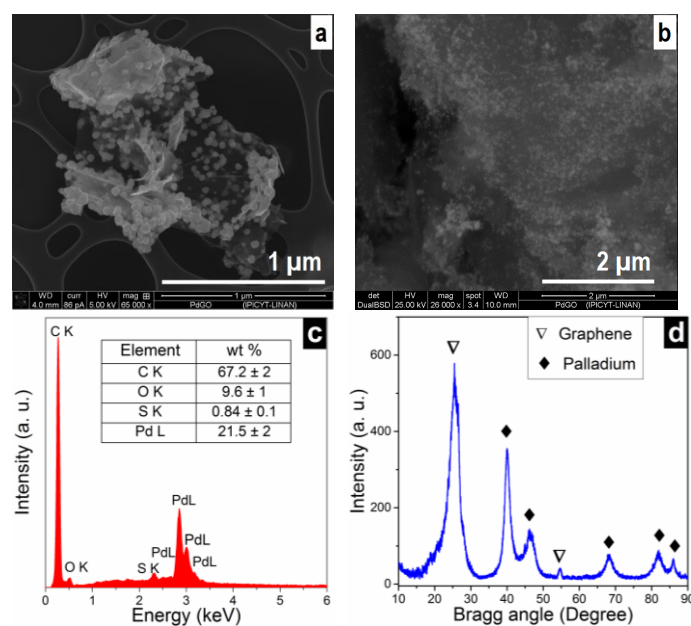


Fig. 3 Electron microscopy images of the as-obtained PdGO nanostructure. (a) Morphological SEM image. (b) Backscattering SEM image. (c) Resulting EDX spectra of the sample and (d) Corresponding XRD pattern.

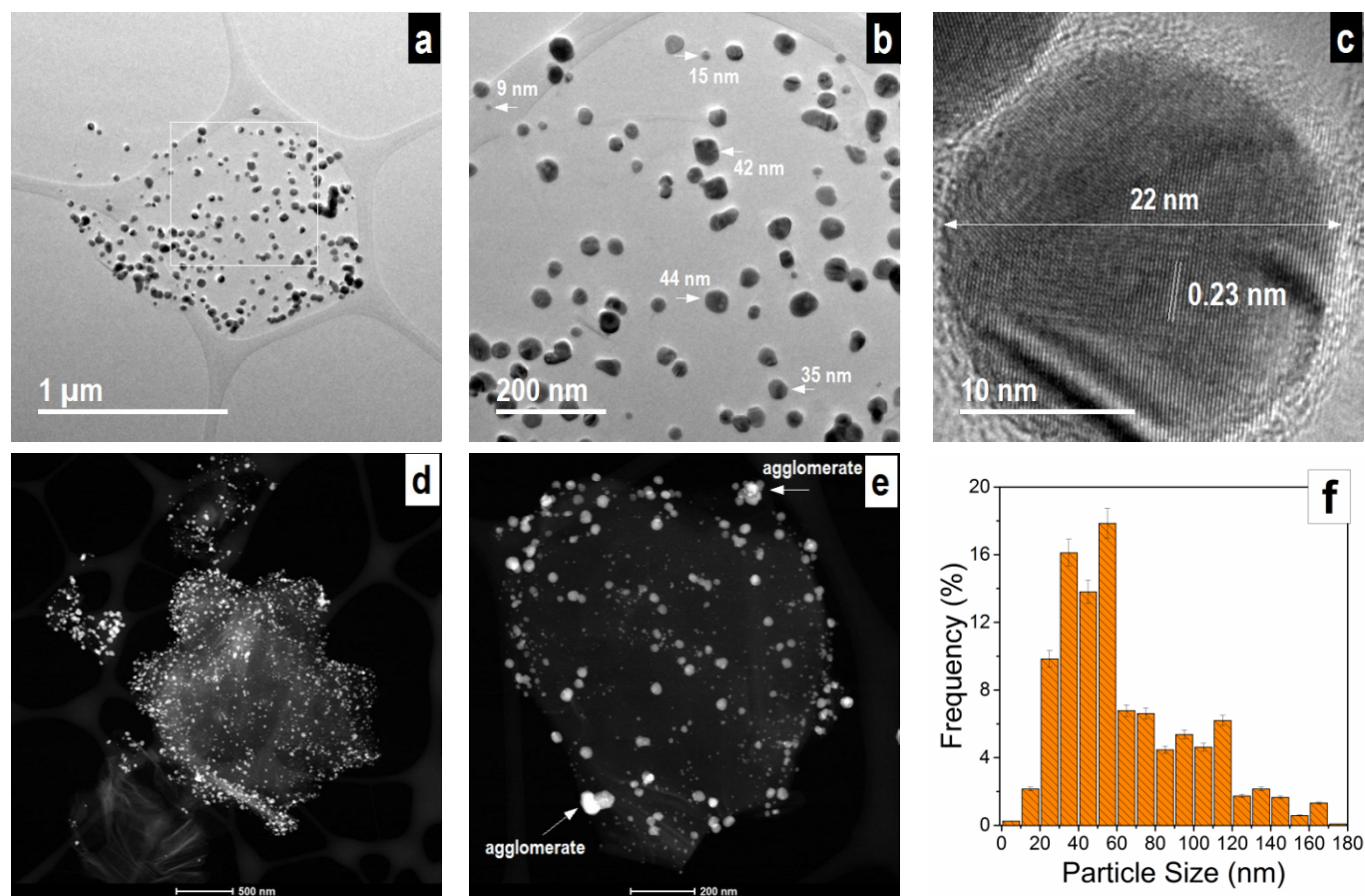


Fig. 4 (a, b) Low and high magnifications of TEM images of as-synthesized PdGO supported on a lacy carbon copper grid. (c) Selected HR-TEM image of a single palladium nanoparticle showing the fringe planes (111). (d, e) HAADF-STEM images of PdGO showing the distribution of PdNPs, and (f) their corresponding palladium size distribution.

Figure 4 shows TEM analyses of the synthesized PdGO. Figure 4a shows a flat and transparent sheet of graphene with scarce wrinkling and highly decorated with dispersed palladium nanoparticles. As it was mentioned above, the employed methodology for preparing PdGO allows the successful exfoliation of graphene layers. This phenomenon results from the induced effect between microwave-induced expansion and gaseous products from the decomposition of EMIM-BF₄ and Pdacac to obtain very thin graphene layers. A close-up of this image shows that these PdNPs are homogeneously anchored with resulting size ranging from 9 to 44 nm (Fig. 4b). High-resolution TEM (HRTEM) shows an individual PdNP with a size of 22 nm, where a well-ordered interplanar spacing with a crystal lattice of 2.3 Å is visible, corresponding to the (111) lattice fringes of Pd.³⁴ Also, it can be seen in this image that the thin graphene layers are capable of wrapping PdNPs. In order to analyze the size distribution of PdNPs, we carried out the HAADF-STEM analysis. The Z contrast allows a better observation of the PdNPs anchored on graphene. As shown in Fig 4d and 4e, the PdNPs appear brighter than the graphene layers and the average size of these nanoparticles is between 40

and 50 nm as it can be seen in the corresponding histogram in Figure 4f. The slight differences between the XRD and HAADF-STEM can be explained on the basis that these two methods provide different information about particle sizes. The XRD analysis gives an average volume measurement which refers to the material crystallite sizes. Conversely, the TEM measurement provides real information of particle size distributions. In this case, both XRD and HAADF-STEM results are similar. The HAADF-STEM images also reveal the presence of agglomerates-nanoparticles. This anomaly can be attributed to the occurrence of defects and functional groups during the synthesis of PdGO, which facilitates the nucleation and agglomeration of these PdNPs. In all cases, we observe that the nanoparticles are dispersed on the graphene layers, which have sizes in the micrometer range.

3.2 Sensor fabrication and electrical response

Prototype sensors were prepared by drop-casting to make electrical contact between the electrodes; once the active layers are dried, the sensors are obtained. Figure 5a shows an image of the as-prepared device. These sensors were typically built from graphene

layers of different sizes, shapes and thicknesses, which randomly overlapped. Since the layers sizes are not uniform and their contacts are random, differences in electrical properties can occur. Also, structural graphene features can produce re-stacking or even agglomeration of exfoliated layers when dried due to π - π interactions. On the other hand, it has been reported recently that the voltage applied to sensors can lead to major defects on the active layers, increasing their resistance due to Joule heating which leads to a similar oxidation process,³⁵ making it difficult to have reproducibility. In order to avoid unwanted signals, we analyzed the bias-voltage effect in our sensor. According to our results, these sensors show a good-lineal-electrical response and we choose 1 V as a bias voltage. As shown in Figure 5b, these devices feature a lineal behavior which indicates good ohmic contact. This result indicates that the deposited film maintains good surface contact on the electrodes.

3.3 Sensing measurements

Detection of hydrogen gas was carried out by measuring the impedance response (Z) of the prototype sensors, and the real part is reported as (R). Alternating the H_2 exposure in the sensor atmosphere induces a resistance response variation, which corresponds to the sensor sensitivity (S). S is defined as the relative resistance change (or Z) in the presence of hydrogen at the initial resistance (R_a) if only air is applied under bias voltage and it is calculated by the following equation:

$$S(\%) = \frac{(R_g - R_a)}{R_a} * 100 \quad (1)$$

The sensor sensitivities at six different H_2 concentrations are shown in Figure 6a and summarized in Figure 6b. The mixture conditions of the used gases and equivalent hydrogen concentrations in ppm and vol. % can be seen in the Table S1 (Supporting Information). According to these results, the relationship between the sensor response and the H_2 concentration is not completely lineal. As it can be seen, at low hydrogen concentrations (up to 1 vol. %) a linear correlation can be found, but this behavior changes with increased concentration until reaching saturation.

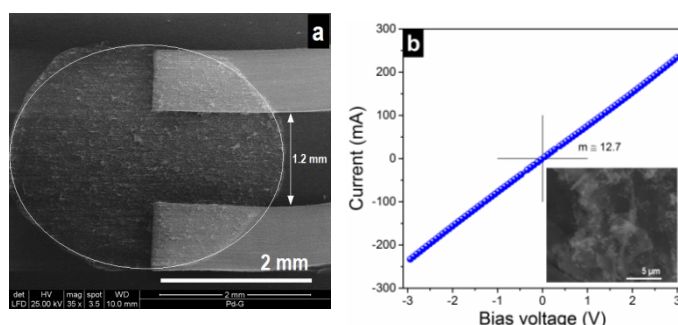


Fig. 5 (a) Image of the as-fabricated hydrogen sensors, PdGO thin films as-deposited on a glass substrate between two copper contacts. (b) Characteristic I-V curve of the performed tests which shows a linear response.

A common approach to explain this behavior is Sievert's law, which states that the solubility of a diatomic gas in a metal is proportional to the square root of the partial pressure of the gas at thermodynamic equilibrium.³⁶ Sieverts law is valid at very low hydrogen concentrations in Pd, mostly applicable at up to 1 vol. % (10000 ppm) in Pd- H_2 systems. The inset in Fig 6b shows the sensor response as a function of the square root of the H_2 concentration with good agreement between the experimental data and Sievert's law. Also, this law explains the characteristic behavior of hydrogen adsorption on a palladium surface in the analyzed concentration range during detection. Hydrogen detection with graphene only as active layer shows negligible response (results not shown); therefore, palladium is the catalytic component that plays a vital role in detection. At room temperature, the attained adsorption equilibrium in the Pd- H_2 systems is determined by the surface reaction, and resistance changes are due to the hydrogen absorption and desorption on PdNPs for the case of a diffusion controlled reaction. A possible reaction mechanism during hydrogen detection can be written as:³⁷



The fraction of free sites (ϑ) may be derived from Langmuir isotherm, thus, the adsorption (r_a) and desorption (r_d) rates of hydrogen molecules can be expressed as:³⁸

$$r_a = k_a C(1 - \vartheta)^2, \quad r_d = k_d \vartheta^2 \quad (3)$$

where k_a and k_d are the adsorption and desorption constants, respectively. C is the hydrogen concentration and ϑ is the fraction of free sites for hydrogen adsorption.

In hydrogen absence, the surface fraction occupied by hydrogen molecules is negligible (i.e. $1 - \vartheta \approx 1$), so the initial detection response is linearly related to the hydrogen concentration. When hydrogen concentration increases, the detection response declines as $(1 - \vartheta)^2$ because the surface fraction is quickly occupied until reaching its maximum value ($\vartheta = 1$). At this point, the sensor sensitivity reaches its saturation level, which indicates a limited number of PdNPs on PdGO composite. Adsorption and desorption rates are dependent on both the hydrogen concentration as well as the fraction of free sites, where r_a is a function of the hydrogen pressure and hydrogen concentration and r_d is only a function of the hydrogen concentration.³⁷ Once the sensor sensitivity reaches its saturation level, the surface fraction sites reach their maximum occupation value, and the initial desorption and recovery rates are high due to the relative high value of ϑ^2 , which gradually falls down as the hydrogen desorption continues. The aforesaid produces the typical curve of the recovery response known as shark fin.³⁹ The evaluated PdGO sensors show a fast signal detection and recovery behavior, which are attributed to a fast kinetics of adsorption and desorption of hydrogen molecules on the limited density of active sites (PdNPs) of the sensor. Also, the sensor exhibits a square shape of the detection responses rather than the shark fin, such results are similar to those reported by Pak et al.,³⁹ which suggest the presence of highly conductive graphene layers because they used CVD-grown graphene.

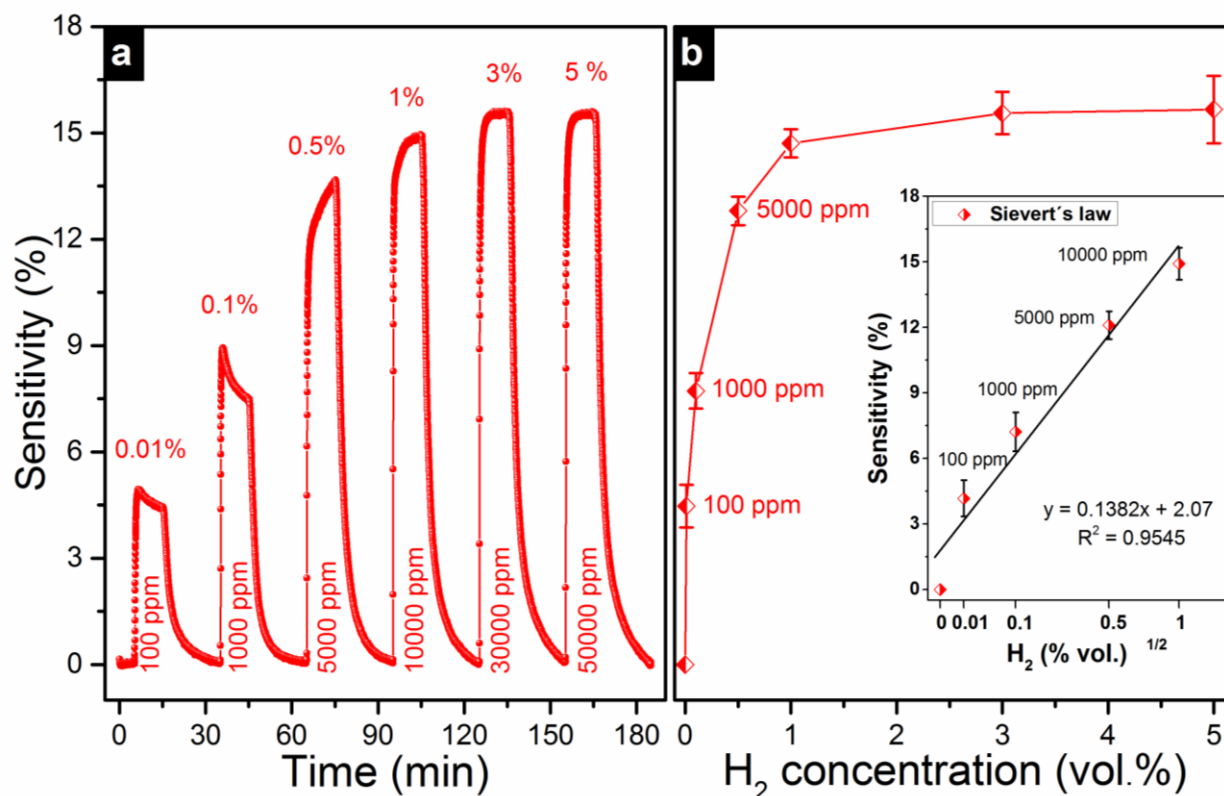


Fig. 6 (a) Sensitivity responses of H₂ detection in air stream for different concentrations (0.01-5 vol. %) at room temperature. (b) Behavior of the sensor sensitivity at different concentrations, the inset is a H₂ response according to Sievert law.

Figure 7 shows the hydrogen-detection response for a palladium-graphene-resistive-type sensor at different concentrations for six consecutive hydrogen injections. When H₂ was released into the air stream, a fast change in the resistance response is observed until reaching a saturation value, which depends on the hydrogen concentration. When the H₂ flow is removed from the gas stream and only synthetic air is flowing, the resistance value recovers its initial value and returns to the initial baseline. All hydrogen-detection responses obtained with Pd-graphene sensors, showed a highly stable and reproducible response at different concentrations for consecutive H₂ injections over a time period of 3 h. In general, this sensor response exhibited an increase in the measured impedance (ΔR) with increasing H₂ concentrations, which is consistent with other works.³⁹⁻⁴¹

The sensor sensitivity shows that with different hydrogen concentrations, sometimes, the detection signals still rise or fall slowly. This is attributed to the time necessary for establishing a stable flow, because when the control valve was opened and hydrogen gas was injected into the air stream, a smooth transition towards a steady flow occurred. This phenomenon is more visible at low hydrogen concentrations and may cause errors in the detected concentration when the saturation time is not reached. To verify our results, we carried out the hydrogen detection with longer detection times with similar behaviors (Fig. S4, Supporting

Information), indicating that the time of 10 min, for detection, and 20 min, for recovery, are adequate to observe the reliable detection signals of the as-prepared sensor. Furthermore, the results indicate that the pressure used during the detection tests exerts a paramount influence over the output detection signal. Very few studies on H₂ detection specify the pressure used during the experimental tests. In order to maintain the same experimental conditions, we chose a pressure of 1 bar.

In addition, not appreciable baseline shift in the sensor response between each consecutive H₂ injection was observed within the studied concentration range, as it can be seen in the raw data detection (Fig. S5, Supporting Information). For example, García-Aguilar *et al.* reported a similar work but the response of the sensor diminished progressively for the next switches.²⁰ The reproducibility of these results was carried out by comparing with other sensor samples at the same different H₂ concentrations with similar results, which demonstrates that in all hydrogen-detection, the sensitivities of the samples have reliable, reproducible and fast response signal detections (Fig. S6 and Table S2, Supporting Information). The difference in the detection results can be attributed to the different amounts of surface adsorption sites (PdNPs). At 3-5 vol. %, the sensor response saturates, creating differences in detection, mostly at 5 vol. % due to this effect.

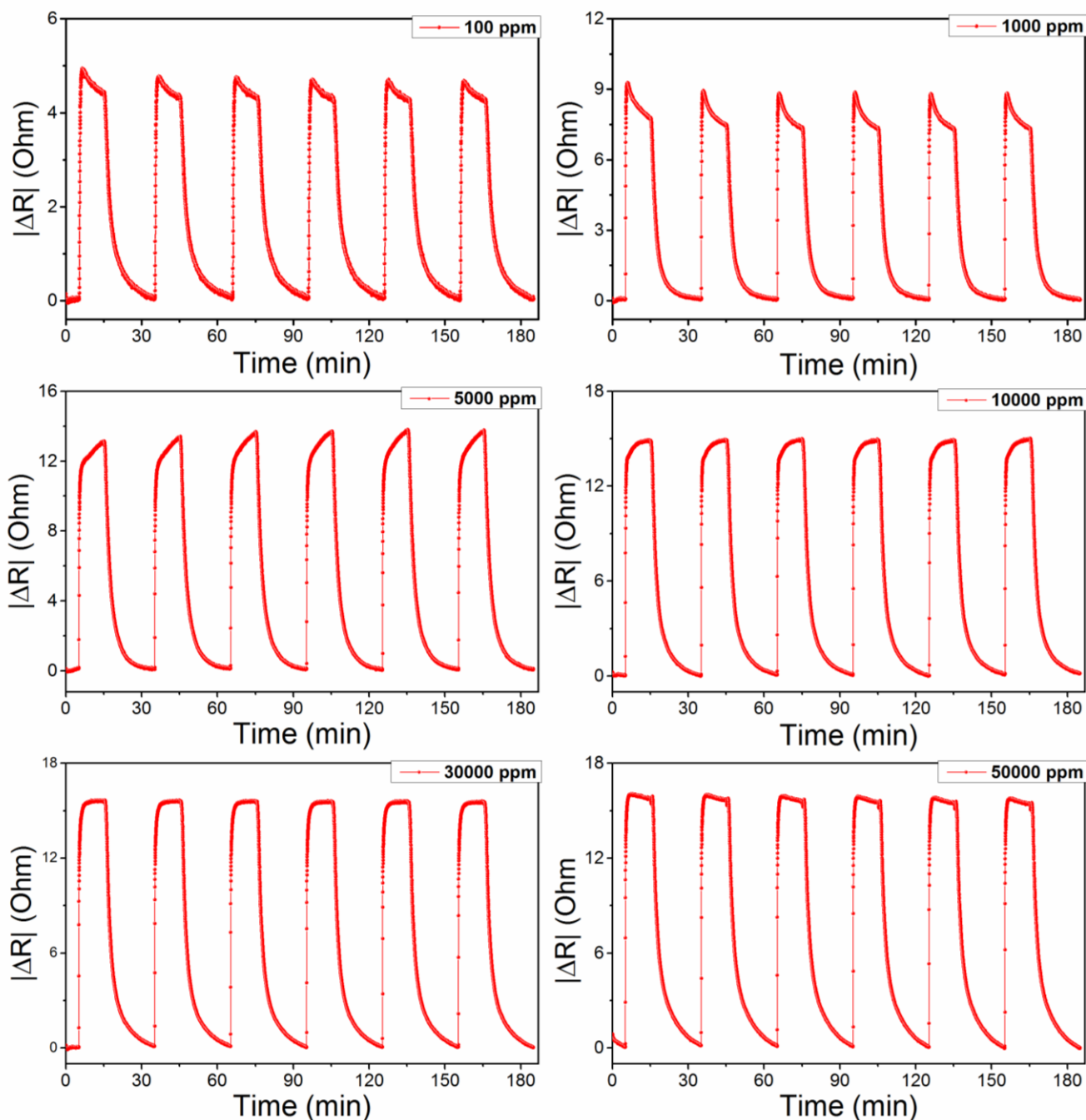


Fig. 7 Response of hydrogen detection diluted in air at different concentrations (100-50000 ppm) at room temperature. The test sequence was performed with six detection times which show signal reproducibility. The duration of each step was 10 min for detection and 20 min for recovery.

In most applications where the use of a hydrogen sensor is required, it must respond quickly. Two commonly evaluated parameters in this regard are the response and recovery times. The response time is determined by the diffusion length of molecular hydrogen into the air stream, from the opening control valve to the sensing chamber. In our experiments, this time was found to be

below 1 min (~40 seg) for all the analyzed samples. However, if we do not consider the diffusion-path of hydrogen and only the obtained experimental data are analyzed, Figure 8 is obtained, which shows the response (90% of its saturated values) and recovery times (90% of total change) at different hydrogen concentrations.

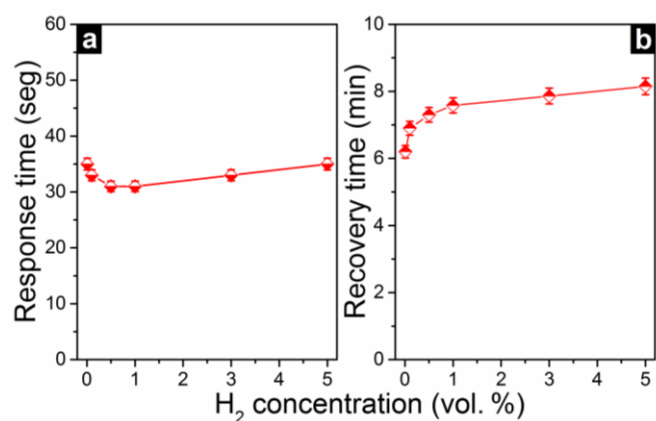


Fig. 8 (a) Results of response time and (b) recovery time for the sensor prototype prepared at different H₂ concentrations analyzed at room temperature.

The response time for this device is always below 1 min (30–35 s) for all the tested hydrogen concentrations. Initially, we observed a slight decrease in response time from 35 s to 30 s, but when H₂ concentrations increased, the response time decreases and returned to the initial value (35 s). This response time slightly changes between different as-prepared sensors, but it does not change significantly, being less than 1 min. As for the recovery time it can be seen that this parameter has a value that is lower than 8 min; at low concentrations, it took 6 min to reach 90% of its saturated value. The recovery time increases as the H₂ concentration increases, reaching 8 min for the highest concentration (5 vol. %, 50000 ppm). These results demonstrate an excellent response and recovery times, which are attributed to the well dispersed Pd-NPs, anchored on well reduced and conductive graphene layers, which facilitate the gas adsorption and desorption. The obtained response and recovery times have similar values or even lower than those found in other similar works.^{20,39–41}

3.4 Sensing mechanism

The as-prepared sensors are resistive-type sensors, which consist of a conductive platform (graphene) and a catalytic component (Pd). During hydrogen-detection, graphene acts primarily as a conductive path between the electrodes, which function as source and drain. This is because H₂ is a nonpolar molecule and its interaction with graphene-based systems is governed by weak dipolar forces called London forces,⁴² while the interaction of hydrogen with transition metals, such as Pd, allows the adsorption and dissociation of hydrogen molecules.^{42,43} So, the adsorption of hydrogen molecules on PdNPs induces charge transfer, from gas molecules to graphene layers, resulting in a resistance change (or impedance) of the sensor. The increase in hydrogen-induced resistance is due to the formation of a palladium hydride. When hydrogen molecules reach the PdNPs anchored on graphene layers, the work function of Pd decreases due to the formation of dipoles (H₂ dissociative adsorption) on the palladium surface, changing the energy that an electron needs to leave the palladium particles.⁴⁴ Hence, the electrons are transferred to graphene, depleting the major graphene holes carriers and thus, increasing the resistance measurements. So, the main mechanism is attributed to the reversible absorption of H₂ in PdNPs.¹⁰

Although it has been reported that functional groups present in graphene can contribute to the sensor response,¹⁹ we considered that this effect is associated with the polarity of the gas to be detected. On the other hand, gaseous adsorbates with different structures and compositions interact with the palladium nanoparticles or graphene layers in distinct ways. At this point, it should be added that the functional groups play an important role in detecting gases by facilitating the interaction with the gas molecules to be detected, but the control of the electrical conductivity is also important, especially, when the sensors are based on conductivity or resistance changes because functional groups may compromise the sensor electrical transport. Ideally, it is desirable to have the catalytic component (Pd) well dispersed in an electrically conductive support to reduce the ohmic resistance and facilitate the charge transfer. A proposed scheme of hydrogen absorption and desorption on PdNPs as main mechanism of hydrogen detection is shown in Figure 9.

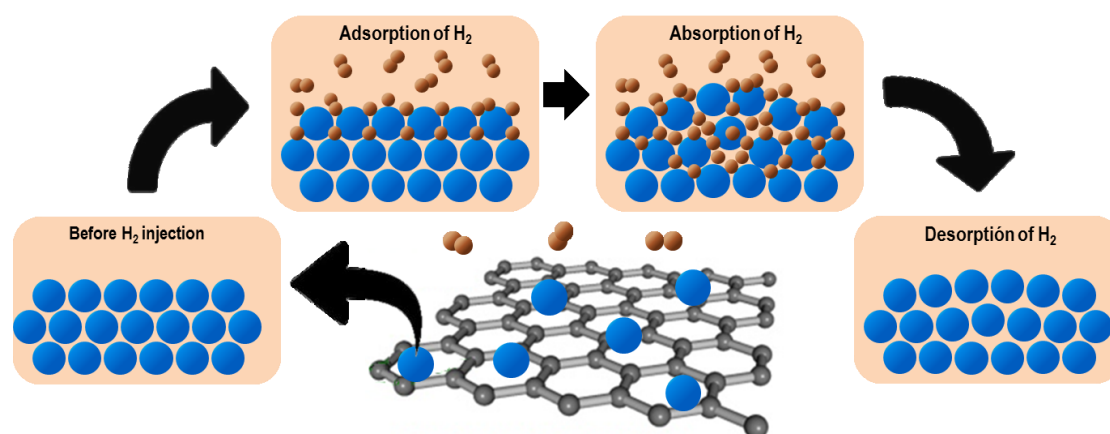


Fig. 9 Schematic representation of the proposed hydrogen adsorption and desorption on palladium nanoparticles as principal mechanism of hydrogen detection with PdGO sensors at room temperature. When hydrogen concentration increases, it can cause structural changes in the palladium after hydrogen desorption.



NJC

PAPER

A comparison of the results with other Pd-based sensors seems interesting, but this comparison can only be relative because the experimental conditions are different. García-Aguilar et al.²⁰ show the results of six cycles of hydrogen detection (only 3.3 vol. % in air) with Pd-SWCNTs, but their raw data of the sensor response diminishes between each detection cycle until no resistance change was detected. This resistance decrease is not desirable regarding the reproducibility, and the resistance values of their sensors are in the range of Mohms, which turns these measurements less precise. Duy-Thach et al.⁴⁰ investigated the hysteresis behavior in Pd-RGO sensors by incorporating Ni (1, 7 and 21 wt. %) for hydrogen detection, with better results at 7 wt. % of Ni. In another paper by Duy-Thach, the effects of Pd nanocubes size on H₂ sensing for the Pd nanocube-graphene hybrid are reported.⁴⁵ Their experimental results show the characteristic shark-fin response and recovery curve, indicating a slow H₂ adsorption and desorption kinetics. We believe that this is due to defects in the RGO layers given the typical shark fin response and resistance values of the sensors (1-4 Kohms). Pak et al. communicated the detection of H₂ in a N₂ stream with sensors prepared from Pd-decorated-graphene nanoribbons, which was synthesized by CVD.³⁹ The sensitivity values of their sensors are similar to our results, suggesting that the resistance in this type of sensor is critical because defects and remaining functional groups on the reduced graphene oxide may compromise the sensor electrical transport. That is, for hydrogen detection with Pd-graphene nanocomposites, where Pd acts as the main catalytic component for the detection, it is desirable to have this catalytic component well dispersed in an electrically conductive path with less electrical noise, in order to obtain a fast adsorption and desorption gas kinetics and to reduce the ohmic resistance which facilitates the charge transfer.

4. Conclusions

Highly-exfoliated-graphene layers functionalized with palladium nanoparticles were successfully produced by the hydrothermal-microwave exfoliation method. Gas-sensor prototypes for H₂ sensing were made with as-synthesized-palladium-graphene nanostructures. The test results show a promising detection response in a wide range of H₂ concentration from 0.01 vol. % (100 ppm) to 5 vol. % (50000 ppm) under ambient air conditions. The prototype sensors exhibited a very reproducible performance with fast response times (~30 s) and recovery properties at room temperature attributed to the well-dispersed-catalytic component (Pd) in a highly-electrically conductive path (graphene layers), which reduce the ohmic resistance and facilitate the charge transfer when hydrogen is exposed. Our results show that it is feasible to obtain an efficient H₂ sensor with reliable and reproducible sensing properties by means of a simple and cost-effective preparation

method under real atmospheric conditions. Furthermore, the control of the electrical conductivity is important for resistive-type sensors.

Acknowledgements

We gratefully acknowledge G. Labrada Delgado, B. Rivera Escoto, Iris Peña Maldonado, H. Gabriel Silva and Dulce Partida from LINAN-DCA-IPICYT, for their assistance with the characterizations. We thank CONACYT for the financial support provided through the SEP CONACYT-2014 S-2780 project. R.D. Martínez-Orozco appreciates the PhD scholarship granted by CONACYT.

References

- 1 C.-J. Winter, *Int. J. Hydrogen Energy*, 2009, **34**, S1–S52.
- 2 M. Balla and M. Wietschel, *Int. J. Hydrogen Energy*, 2009, **34**, 615–627.
- 3 S. K. Arya, S. Krishnan, H. Silva, S. Jeana and S. Bhansali, *Analyst*, 2012, **137**, 2743–2756.
- 4 B. Wang, L. F. Zhu, Y. H. Yang, N. S. Xu and G. W. Yang, *J. Phys. Chem. C*, 2008, **112**, 6643–6647.
- 5 A. Qurashia, E. M. El-Maghraby, T. Yamazakia and T. Kikuta, *Sensor Actuators B*, 2010, **147**, 48–54.
- 6 S. Öztürk, N. Kılıç, İ. Torun, A. Kösemen, Y. Şahin and Z. Z. Öztürk, *Int. J. Hydrogen Energy*, 2014, **39**, 5194–5201.
- 7 P.-C. Chou, H.-I. Chen, I.-P. Liu, C.-C. Chen, J.-K. Liou, K.-S. Hsu and W.-C. Liu, *Int. J. Hydrogen Energy*, 2015, **40**, 729–734.
- 8 C. Lu and Z. Chen, *Sensor Actuators B*, 2009, **140**, 109–115.
- 9 T. B. Flanagan, *Annu. Rev. Mater. Sci.*, 1991, **21**, 269–304.
- 10 E. Lee, J. M. Lee, J. H. Koo, W. Lee and T. Lee, *Int. J. Hydrogen Energy*, 2010, **35**, 6984–6991.
- 11 F. Yang, D. K. Taggart and R. M. Penner, *Small*, 2010, **6**, 1422–1429.
- 12 K. J. Jeon, J. M. Lee, E. Lee and W. Lee, *Nanotechnology*, 2009, **20**, 135502.
- 13 F. Favier, E. C. Walter, M. P. Zach, T. Benter and R. M. Penner, *Science*, 2001, **293**, 2227–2231.
- 14 S. Yu, U. Welp, L. Z. Hua, A. Rydh, W. K. Kwok and H. H. Wang, *Chem. Mater.*, 2005, **17**, 3445–3450.
- 15 U. Lange, T. Hirsch, V. M. Mirsky and O. S. Wolfbeis, *Electrochimica Acta*, 2011, **56**, 3707–3712.
- 16 J. L. Johnson, A. Behnam, S. J. Pearton and A. Ural, *Adv. Mater.*, 2010, **22**, 4877–4880.
- 17 S. Mubeen, T. Zhang, B. Yoo, M. A. Deshusses and N. V. Myung, *J. Phys. Chem. C*, 2007, **111**, 6321–6327.
- 18 S. Cui, S. Mao, Z. Wen, J. Chang, Y. Zhang and J. Chen, *Analyst*, 2013, **138**, 2877–2882.

- 19 S. Prezioso, F. Perrozzi, L. Giancaterini, C. Cantalini, E. Treossi, V. Palermo, M. Nardone, S. Santucci and L. Ottaviano, *J. Phys. Chem. C*, 2013, **117**, 10683-10690.
- 20 J. García-Aguilar, I. Miguel-García, Á. Berenguer-Murcia and D. Cazorla-Amorós, *Carbon*, 2014, **66**, 599-611.
- 21 C. N. R. Rao, G. U. Kulkarni, P. J. Thomas and P. P. Edwards, *Chem. Eur. J.*, 2002, **8**, 28-35.
- 22 Y. Si and E. T. Samulski, *Chem. Mater.*, 2008, **20**, 6792-6797.
- 23 S. Gadipelli and Z. X. Guo, *Prog. Mater. Sci.*, 2015, **69**, 1-60.
- 24 V. Sridhar, H.-J. Kim, J.-H. Jung, C. Lee, S. Park and I.-K. Oh, *ACS Nano*, 2012, **6**, 10562-10570.
- 25 S.-H. Lee, V. Sridhar, J.-H. Jung, K. Karthikeyan, Y.-S. Lee, R. Mukherjee, N. Koratkar and I.-K. Oh, *ACS Nano*, 2013, **7**, 4242-4251.
- 26 D. C. Marcano, D. V. Kosynkin, J. M. Berlin, A. Sinitskii, Z. Sun, A. Slesarev, L. B. Alemany, W. Lu and J. M. Tour, *ACS Nano*, 2010, **4**, 4806-4814.
- 27 L. Wu, L. Liu, B. Gao, R. Muñoz-Carpena, M. Zhang, H. Chen, Z. Zhou and H. Wang, *Langmuir*, 2013, **29**, 15174-15181.
- 28 G. Eda, J. Ball, C. Mattevi, M. Acik, L. Artiglia, G. Granozzi, Y. Chabal, T. D. Anthopoulos and M. Chhowalla, *J. Mater. Chem.*, 2011, **21**, 11217-11223.
- 29 K. N. Kudin, B. Ozbas, H. C. Schniepp, R. K. Prud'homme, I. A. Aksay and R. Car, *Nano Lett.*, 2008, **8**, 36-41.
- 30 Y. Si and E. T. Samulski, *Nano letters*, 2008, **8**, 1679-1682.
- 31 S. Stankovich, R. D. Piner, S. T. Nguyen and R. S. Ruoff, *Carbon*, 2006, **44**, 3342-3347.
- 32 A. Dimiev and J. M. Tour, *ACS Nano*, 2014, **8**, 3060-3068.
- 33 Z.-L. Chen, F.-Y. Kam, R. G. S. Goh, J. Song, G.-K. Lim and L.-L. Chua, *Chem. Mater.*, 2013, **25**, 2944-2949.
- 34 X. Chen, G. Wu, J. Chen, X. Chen, Z. Xie and X. Wang, *J. Am. Chem. Soc.*, 2011, **133**, 3693-3695.
- 35 S. Cui, H. Pu, E. C. Mattson, Z. Wen, J. Chang, Y. Hou, C. J. Hirschmugl and J. Chen, *Anal. Chem.*, 2014, **86**, 7516-7522.
- 36 A. Caravella, F. Scura, G. Barbieri and E. Drioli, *J. Phys. Chem. B*, 2010, **114**, 6033-6047.
- 37 W. Auer and H. J. Grabke, *Ber. Bunsen. Phys. Chem.*, 1974, **78**, 58-67.
- 38 R. I. Masel, Wiley, New York, 1996.
- 39 Y. Pak, S.-M. Kim, H. Jeong, C. G. Kang, J. S. Park, H. Song, R. Lee, N. Myoung, B. H. Lee, S. Seo, J. T. Kim and G.-Y. Jung, *ACS Appl. Mater. Interfaces*, 2014, **6**, 13293-13298.
- 40 D.-T. Phan and G.-S. Chung, *Int. J. Hydrogen Energy*, 2014, **39**, 20294-20304.
- 41 D.-T. Phan and G.-S. Chung, *Sensor Actuators B*, 2014, **2014**, 354-360.
- 42 M. Pumera, *Energy Environ. Sci.*, 2011, **4**, 668-674.
- 43 W. Yuan and G. Shi, *J. Mater. Chem. A*, 2013, **1**, 10078-10091.
- 44 P. Y. Yu and M. Cardona, Springer, New York, 2005.
- 45 D.-T. Phan and G.-S. Chung, *Sensor Actuators B*, 2014, **204**, 437-444.

Graphical Abstract

Hydrogen-gas sensors based on graphene functionalized palladium nanoparticles: the impedance response as a valuable sensor evaluationReinaldo David Martínez-Orozco,^{*a} René Antaño-López^b and Vicente Rodríguez-González^a^a*División de Materiales Avanzados, Instituto Potosino de Investigación Científica y Tecnológica, Camino a la Presa San José 2055 Col. Lomas 4a. sección C.P. 78216, San Luis Potosí, S.L.P., México.*^b*Centro de Investigación y Desarrollo Tecnológico en Electroquímica, S.C., Pedro Escobedo, Querétaro, México.*

Palladium-graphene nanostructures were synthesized by hydrothermal-microwave exfoliation method and employed as active layers for hydrogen gas detection.

